Available online at www.eccomasproceedia.org
Eccomas Proceedia COMPDYN (2023) 2038-2049

ECCOMAS
Proceedia

COMPDYN 2023
9th ECCOMAS Thematic Conference on
Computational Methods in Structural Dynamics and Earthquake Engineering
M. Papadrakakis, M. Fragiadakis (eds.)
Athens, Greece, 12-14 June 2023

WORK AND ENERGY COMPONENTS IN MECHANICAL SYSTEMS WITH COMPLEX HYSTERETIC BEHAVIOR

Raffaele Capuano, Nicolò Vaiana, and Luciano Rosati

Department of Structures for Engineering and Architecture, University of Naples Federico II,
Via Claudio, 21, 80125 Naples, Italy
e-mail: raffaele.capuano@unina.it, nicolo.vaiana@unina.it, rosati@unina.it

Abstract. *We compare the results obtained in terms of work and energy components by running several nonlinear time history analyses on Single Degree of Freedom (SDoF) hysteretic mechanical systems under three different conditions: (i) free vibration, (ii) oscillations forced by harmonic load, and (iii) oscillations forced by random load. The nonlinear responses of the SDoF mechanical systems are modeled by using a rate-independent hysteretic element. In particular, to simulate the associated complex generalized force-displacement relations, obtained as combination of asymmetric, flag-shaped, S-shaped, and pinched hysteresis loops, we use a novel uniaxial phenomenological model, denominated Vaiana-Rosati Model (VRM), that employs closed-form expressions to compute the generalized force and work. In addition, to evaluate the time evolution of the generalized work and energy components of the analyzed systems, the general expression of the Modified Work-Energy (MWE) theorem is used.*

Keywords: Complex Mechanical Hysteresis, Hysteretic Mechanical System, Vaiana-Rosati Model, Dissipative Systems, Path-Dependent Work.

ISSN:2623-3347
Peer-review under responsibility of the organizing committee of COMPDYN 2023.
doi: 10.7712/120123.10540.21081

1 INTRODUCTION

Hysteretic mechanical systems and materials, adopted in the field of aerospace, civil, and mechanical engineering, typically exhibit complex hysteresis loop shapes in the input-output plane when cyclic input variables are imposed. A detailed classification has been recently proposed to describe such complex responses. Indeed, as described by Vaiana and Rosati [1], a generalized force-displacement hysteresis loop can be described by means of four different curves, namely the generic loading and unloading curves and the generic upper and lower limiting curves. Consequently, on the basis of the analytical properties of the limiting curves, the hysteresis loops have been classified in [1] into four main categories: (i) hysteresis loops limited by straight lines, (ii) hysteresis loops limited by two curves with no inflection point, (iii) hysteresis loops limited by two curves with one inflection point, and (iv) hysteresis loops limited by two curves with two inflection points. This classification provides valuable insights into different types of response that hysteretic systems and materials provide to external forces and displacements.

The amount of mechanical energy dissipated by non-conservative forces plays a crucial role in the evaluation of work and energy components in the context of hysteretic mechanical systems and materials [2]. Actually, the study of these complex responses provides crucial information on the system behavior, what can be adopted for both analysis and design purposes. As an example, such a information is essential to understand how hysteretic mechanical systems and materials react to external influences, leading to accurate prediction of their performance under various conditions.

The uniaxial phenomenological model proposed by Vaiana and Rosati [1] is a powerful tool for simulating the complex behavior of hysteretic mechanical systems and materials. This model has been selected due to its capability to accurately capture rate-independent hysteretic responses, including symmetric, asymmetric, pinched, S-shaped, or flag-shaped hysteresis loops as well as combinations of them. Furthermore, this model offers several advantages over other models available in the literature [3, 4, 5, 6] since it: (i) allows for the modeling of the loading and unloading phases by employing two different sets of eight parameters, (ii) provides closed-form expressions for the evaluation of the generalized force, work, and internal energy change, and (iii) requires parameters having a clear theoretical and/or experimental interpretation. These features are not available in other existing models, at least in a unified manner.

The paper is organized into three parts. In the first part (Section 2), we describe the general classification of hysteresis loops having complex shapes.

In the second part (Section 3), we first describe the formulation of the VRM. Subsequently, for the reader's convenience, we briefly introduce the closed-form expressions for the generalized work done by a generalized rate-independent hysteretic force, simulated by the VRM, over a generic generalized displacement interval.

Finally, in the last part (Section 4), we show the results of several nonlinear time history analyses carried out on two SDoF hysteretic mechanical systems with complex hysteresis loop shapes, in order to clearly analyze their responses in terms of generalized work and energy components.

2 CLASSIFICATION OF COMPLEX HYSTERESIS LOOPS

In the literature, it is now available a detailed and unified classification of the most common types of hysteresis loops characterized by complex shapes for which no cyclic softening/hardening phenomena are present [1]. Based on this classification, the complex response, in the generalized force f and generalized displacement u plane, can be described through the

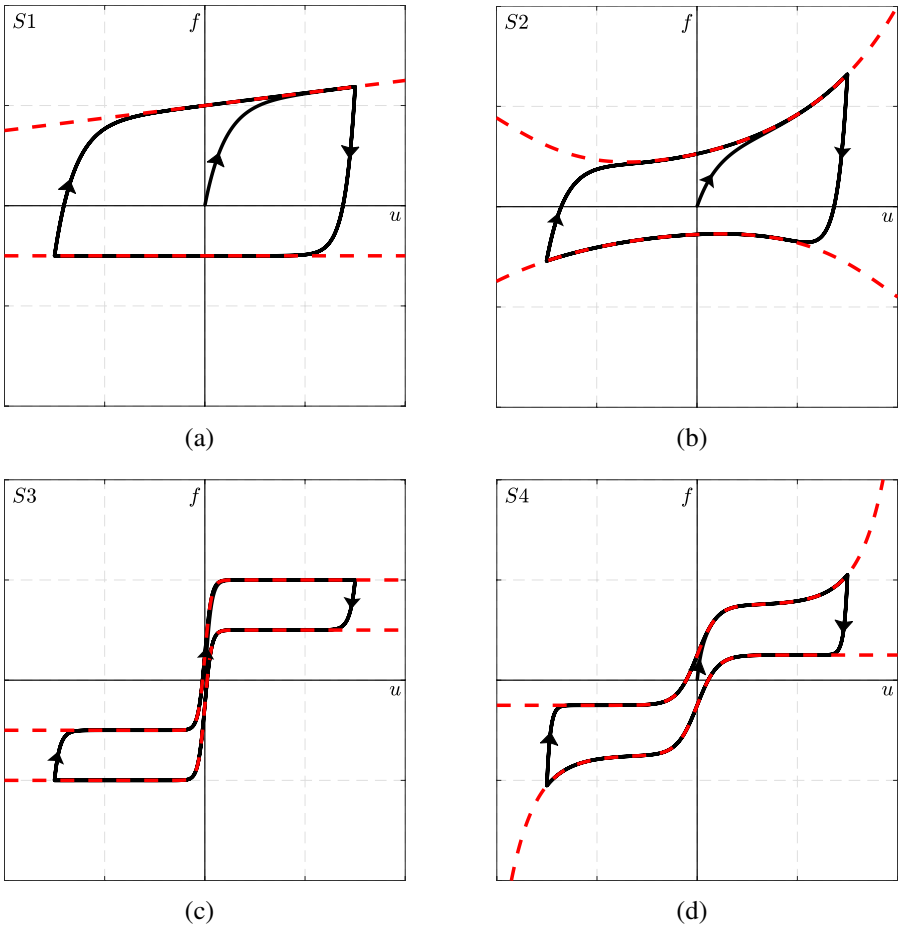

Figure 1: Typical complex hysteresis loops belonging to the shape type categories $S1$ (a), $S2$ (b), $S3$ (c), and $S4$ (d).

use of four curves, namely the loading and unloading curves, as well as the upper and lower limiting curves. According to the analytical properties of the upper and lower limit curves, hysteresis loops can be classified into four main categories:

- shape type $S1$, characterized by hysteresis loops limited by two straight lines (Figure 1a);
- shape type $S2$, characterized by hysteresis loops limited by two curves with no inflection point (Figure 1b);
- shape type $S3$, characterized by hysteresis loops limited by two curves with one inflection point (Figure 1c);
- shape type $S4$, characterized by hysteresis loops limited by two curves with two inflection points (Figure 1d).

To emphasize the large number of behaviors that can be simulated through the VRM, it is important to note that Figure 1a shows a symmetric hysteresis loop limited by two non-parallel straight lines (i.e., shape type $S1$), which is typical of steel dampers [7]. Figure 1b shows an asymmetric hysteresis loop belonging to the shape type $S2$, typical of different types of isolators [8, 9]. Figure 1c shows a symmetric hysteresis loop limited by two parallel curves with one inflection point (i.e., shape type $S3$), typical of SMA helical springs [10]. In conclusion, Figure

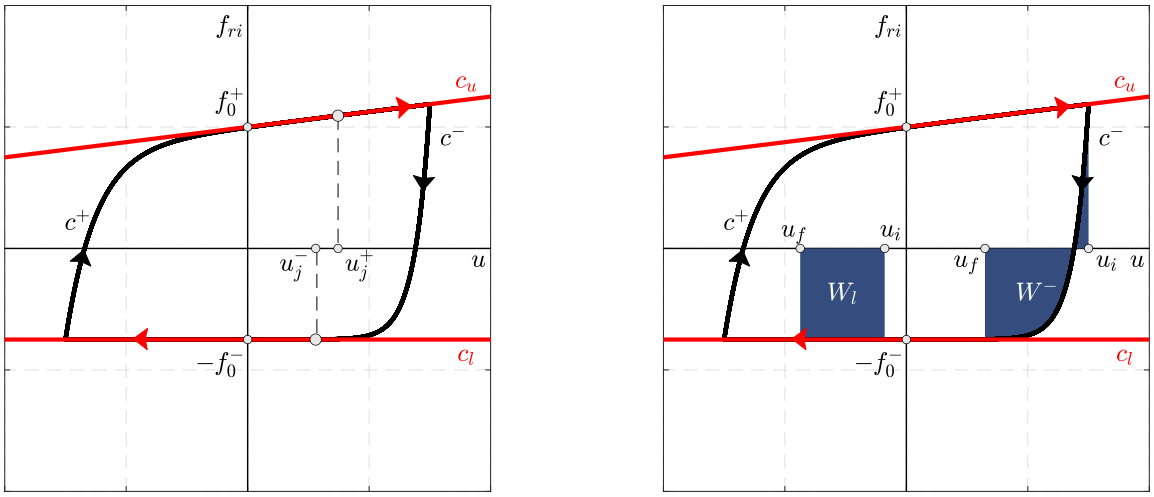

(a) (b)

Figure 2: VRM formulation: curves c^+, c_u, c^-, c_l, (a) and generalized work during a generic unloading phase (b).

1d shows a symmetric hysteresis loop limited by two parallel curves with two inflection points (i.e., shape type $S4$), typical of unbounded fiber reinforced elastomeric bearings [11, 12, 13].

3 VAIANA-ROSATI MODEL

In this section, we first briefly describe the VRM proposed in [1]. This novel uniaxial phenomenological model can accurately simulate a great variety of rate-independent hysteretic responses characterized by symmetric, asymmetric, pinched, S-shaped, flag-shaped hysteresis loops or by a combination of them. Subsequently, we illustrate the closed-form expressions for the generalized work over a generic generalized displacement interval.

3.1 Evaluation of the generalized force

Figure 2a presents a typical hysteresis loop that can be reproduced by means of such a model. In particular, the generalized force f_{ri}, during the generic loading phase ($\dot{u} > 0$), can be evaluated as:

$$f_{ri}(u, u_j^+) = \begin{cases} c^+(u, u_j^+) & \text{when} \quad u < u_j^+ \\ c_u(u) & \text{when} \quad u > u_j^+, \end{cases} \tag{1}$$

whereas, during the generic unloading one ($\dot{u} < 0$), it can be computed as:

$$f_{ri}(u, u_j^-) = \begin{cases} c^-(u, u_j^-) & \text{when} \quad u > u_j^- \\ c_l(u) & \text{when} \quad u < u_j^-. \end{cases} \tag{2}$$

In Equations (1) and (2), c^+ and c^- represent, respectively, the functions associated with the generic loading and unloading curves whose expressions are:

$$\begin{aligned} c^+(u, u_j^+) = \beta_1^+ e^{\beta_2^+ u} - \beta_1^+ + \frac{4\gamma_1^+}{1 + e^{-\gamma_2^+(u-\gamma_3^+)}} - 2\gamma_1^+ + \\ + k_b^+ u + f_0^+ - \frac{1}{\alpha^+}\left[e^{-\alpha^+\left(+u-u_j^+ + \bar{u}^+\right)} - e^{-\alpha^+ \bar{u}^+}\right], \end{aligned} \tag{3}$$

$$c^-(u,u_j^-) = \beta_1^- e^{\beta_2^- u} - \beta_1^- + \frac{4\gamma_1^-}{1+e^{-\gamma_2^-\left(u-\gamma_3^-\right)}} - 2\gamma_1^- + \\ + k_b^- u - f_0^- + \frac{1}{\alpha^-}\left[e^{-\alpha^-\left(-u+u_j^-+\bar{u}^-\right)} - e^{-\alpha^-\bar{u}^-}\right], \tag{4}$$

whereas c_u and c_l are, respectively, those associated with upper and lower limiting curves having expressions:

$$c_u(u) = \beta_1^+ e^{\beta_2^+ u} - \beta_1^+ + \frac{4\gamma_1^+}{1+e^{-\gamma_2^+\left(u-\gamma_3^+\right)}} - 2\gamma_1^+ + k_b^+ u + f_0^+, \tag{5}$$

$$c_l(u) = \beta_1^- e^{\beta_2^- u} - \beta_1^- + \frac{4\gamma_1^-}{1+e^{-\gamma_2^-\left(u-\gamma_3^-\right)}} - 2\gamma_1^- + k_b^- u - f_0^-. \tag{6}$$

The set of eight parameters controlling the generic loading (unloading) phase are represented by k_b^+, f_0^+, α^+, β_1^+, β_2^+, γ_1^+, γ_2^+, γ_3^+ (k_b^-, f_0^-, α^-, β_1^-, β_2^-, γ_1^-, γ_2^-, γ_3^-). Such parameters need to satisfy the following conditions:

- $f_0^+ > 0$, $\alpha^+ > 0$, $f_0^- > 0$, $\alpha^- > 0$.
- k_b^+, β_1^+, β_2^+, γ_1^+, γ_2^+, γ_3^+, k_b^-, β_1^-, β_2^-, γ_1^-, γ_2^-, $\gamma_3^- \in \mathbb{R}$.

Finally, the expressions of the internal variables u_j^+ and u_j^-, characterizing, respectively, the generic loading and unloading phases, and the internal model parameters $\bar{u}^+$ and $\bar{u}^-$ are reported in [1].

3.2 Evaluation of the generalized work

The closed-form expressions of the generalized work related to the four curves are obtained by recalling Equations (1) and (2) and integrating them over a generic generalized displacement interval. In this way, during the generic loading phase ($\dot{u} > 0$) the generalized work is:

$$W(u,u_j^+) = \begin{cases} W^+(u,u_j^+) & \text{when} \quad u < u_j^+ \\ W_u(u) & \text{when} \quad u > u_j^+, \end{cases} \tag{7}$$

whereas, during the generic unloading one ($\dot{u} < 0$), the generalized work can be computed as:

$$W(u,u_j^-) = \begin{cases} W^-(u,u_j^-) & \text{when} \quad u > u_j^- \\ W_l(u) & \text{when} \quad u < u_j^-. \end{cases} \tag{8}$$

To evaluate the expressions of W^+, W_u, W^- and W_l, it is more convenient to rewrite the expressions of the four curves c^+, c_u, c^- and c_l as the sum of terms that depend upon suitable subsets of the model parameters:

$$c^+(u,u_j^+) = c_a^+\left(\beta_1^+,\beta_2^+\right) + c_b^+\left(\gamma_1^+,\gamma_2^+,\gamma_3^+\right) + c_c^+\left(k_b^+,f_0^+\right) + c_d^+\left(\alpha^+\right), \tag{9}$$

$$c_u(u) = c_a^+\left(\beta_1^+,\beta_2^+\right) + c_b^+\left(\gamma_1^+,\gamma_2^+,\gamma_3^+\right) + c_c^+\left(k_b^+,f_0^+\right), \tag{10}$$

$$c^-(u,u_j^-) = c_a^-\left(\beta_1^-,\beta_2^-\right) + c_b^-\left(\gamma_1^-,\gamma_2^-,\gamma_3^-\right) + c_c^-\left(k_b^-,f_0^-\right) + c_d^-\left(\alpha^-\right), \tag{11}$$

$$c_l(u) = c_a^-\left(\beta_1^-,\beta_2^-\right) + c_b^-\left(\gamma_1^-,\gamma_2^-,\gamma_3^-\right) + c_c^-\left(k_b^-,f_0^-\right). \tag{12}$$

Thus, the expression of W^- can be obtained by integrating Equation (11) over $[u_f, u_i]$:

$$W^- = \int_{u_f}^{u_i} c^-(u,u_j^-)\,du = \int_{u_f}^{u_i}\left(c_a^- + c_b^- + c_c^- + c_d^-\right)\,du = W_a^- + W_b^- + W_c^- + W_d^-, \tag{13}$$

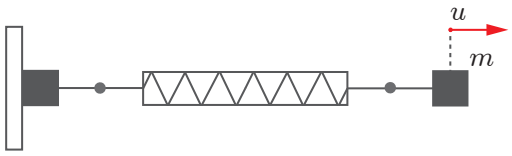

Figure 3: SDoF hysteretic mechanical system.

whereas the one of W_l can be got by integrating Equation (12):

$$W_l = \int_{u_f}^{u_i} c_l(u)\, du = \int_{u_f}^{u_i} \left(c_a^- + c_b^- + c_c^-\right)\, du = W_a^- + W_b^- + W_c^-. \tag{14}$$

Specifically, the terms W_a^-, W_b^-, W_c^-, W_d^- in the previous equations are computed as:

$$W_a^- = \frac{\beta_1^-}{\beta_2^-}\left(e^{\beta_2^- u_f} - e^{\beta_2^- u_i}\right) - \beta_1^-(u_f - u_i), \tag{15}$$

$$W_b^- = 2\gamma_1^- \left\{ \frac{2\ln\left[e^{-\gamma_2^-(u_f-\gamma_3^-)}+1\right]}{\gamma_2^-} - \frac{2\ln\left[e^{-\gamma_2^-(u_i-\gamma_3^-)}+1\right]}{\gamma_2^-} + (u_f - u_i) \right\}, \tag{16}$$

$$W_c^- = \frac{k_b^-}{2}(u_f^2 - u_i^2) - f_0^-(u_f - u_i), \tag{17}$$

$$W_d^- = -\frac{1}{(\alpha^-)^2}\, e^{-\alpha^-(\bar{u}^- + u_j^-)} \left[\alpha^-(u_f - u_i)e^{+\alpha^- u_j^-} - e^{+\alpha^- u_f} + e^{+\alpha^- u_i}\right]. \tag{18}$$

W^- and W_l whose mechanical meaning is associated, respectively, with the area underlying the curves c^- and c_l, over a generic generalized displacement interval $[u_f, u_i]$ are shown in Figure 2b.

Similarly, the expressions of W^+ and W_u are obtained by integrating Equations (9) and (10) over the generalized displacement interval $[u_i, u_f]$; the relevant expressions for the terms W_a^+, W_b^+, W_c^+, W_d^+ are omitted for brevity and can be found in [2].

4 NUMERICAL APPLICATIONS

In this section, we present the comparison of the results obtained by the numerical analyses performed on two SDoF hysteretic mechanical systems in which the nonlinear responses are modeled by means of a rate-independent hysteretic element and using the VRM; the analyses are performed for three specific conditions: (i) free vibration, (ii) oscillations forced by a harmonic load, (iii) oscillations forced by a random load. Specific attention is paid to the evolution of the various components of generalized work and energy components once a steady-state condition, in the case of harmonic force, is reached by the system.

4.1 Analyzed hysteretic mechanical systems

The selected general family of Single Degree of Freedom (SDoF) hysteretic mechanical systems is illustrated in Figure 3. Such a model is composed of a mass m connected to a rate-independent hysteretic spring.

In particular, two hysteretic mechanical systems are selected: the first with hysteretic behavior shown in Figure 4a characterized by an asymmetric flag-shaped hysteresis loop, and belonging to $S3$ category (system A). The second hysteretic mechanical system with hysteretic

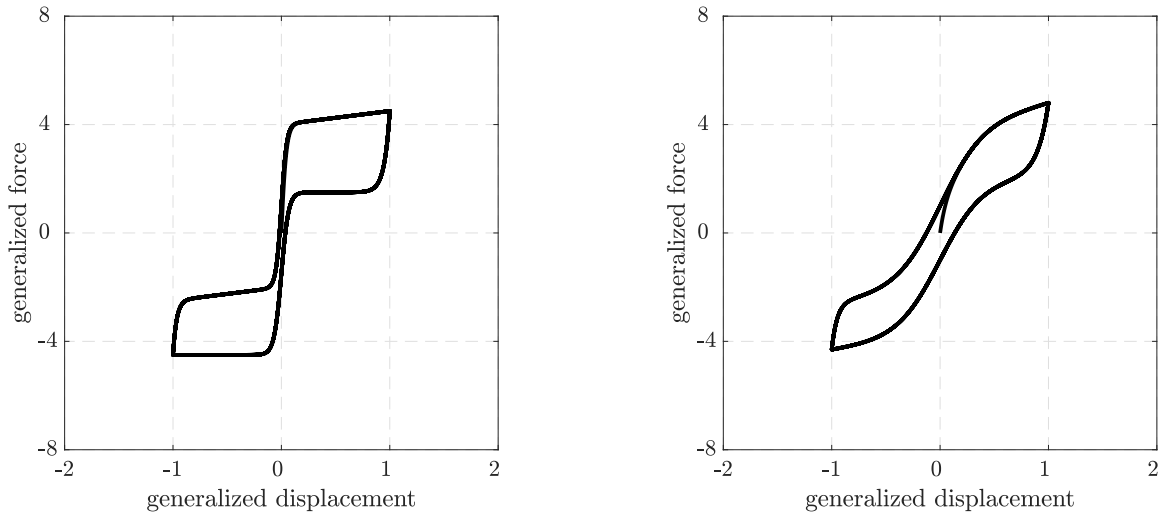

(a) (b)

Figure 4: Complex hysteretic behavior charactering system A (a) and system B (b) simulated by using the VRM parameters in Table 1.

behavior shown in Figure 4b, characterized by an asymmetric S-shaped hysteresis loop with pinching and belonging to $S4$ category (system B). Finally, the loops in Figure 4 are simulated using VRM by employing the parameters listed in Table 1.

Figure	$\mathrm{sgn}(\dot{u})$	k_b	f_0	α	β_1	β_2	γ_1	γ_2	γ_3
4a	$+$	0.5	1.0	30	0.0	0.0	1.5	40	0.0
	$-$	0.0	1.5	20	0.0	0.0	1.5	30	0.0
4b	$+$	0.5	1.0	20	0.2	1.0	1.5	5.0	0.0
	$-$	0.0	1.0	10	-0.2	-1.0	1.5	5.0	0.0

Table 1: VRM parameters adopted to simulate the hysteresis loops in Figure 4.

4.2 Equation of motion

Denoting by u, $\dot{u}$ and $\ddot{u}$ the generalized displacement, velocity, and acceleration, respectively, the equation of motion for the general family of SDoF hysteretic mechanical systems illustrated in Figure 3, can be easily obtained from Newton's second law as:

$$m\ddot{u} + f_{ri}\left(u\right) = p\left(t\right), \tag{19}$$

where f_{ri} is the generalized rate-independent hysteretic force exerted on the rate-independent hysteretic element, assumed to be a function of the generalized displacement u and simulated by using the VRM. Furthermore, p is the time-dependent generalized external force acting on the mass.

4.3 Modified Work-Energy theorem

As shown in [2], the general expression of the Modified Work-Energy (MWE) theorem states that the sum of the generalized mechanical and internal energy variations of a system is equal

to the work done by the generalized external forces acting on the system:

$$\Delta E_M + \Delta E_I = W_p, \tag{20}$$

where the generalized mechanical energy E_M is equal to the sum of the generalized kinetic E_K and potential E_P energies of the system.

With respect to the hysteretic mechanical system shown in Figure 3, there are no generalized conservative forces so that the generalized potential energy is equal to zero. On the other hand, we know that the variation of the generalized internal energy ΔE_I is related to the generalized work of the non-conservative internal forces W_{nc}^i, that in the general family of mechanical systems under consideration, is represented by the work W_{ri} performed by the generalized force exhibited by the rate-independent hysteretic element; hence, it is possible to write:

$$\Delta E_I = -W_{nc}^i = -W_{ri}. \tag{21}$$

On the other hand, W_p in Equation (20), is the generalized work done by the generalized external force $p(t)$ on the mass m. These quantities can be computed as follows:

$$W_{ri} = -\int_{u_i}^{u_f} f_{ri}(u)\, du, \quad W_p = \int_{u_i}^{u_f} p(t)\, du. \tag{22}$$

In particular, W_{ri} can be computed in a closed-form for any generalized displacement interval (Section 3), whereas W_p can be evaluated numerically.

4.4 Integration method and specifications

The response of the systems is evaluated by using an explicit, accurate, and computationally efficient time integration method, described in [14], using a time step $\Delta t = 0.001$ s and a unitary mass. The hysteretic model and the solution algorithm have been programmed in MATLAB R2022b and run on a computer having an Intel Core i5 dual-core processor and a CPU at 2.30 GHz with 8 GB of RAM.

4.5 Numerical Results

4.5.1 Free vibrations

To evaluate the free vibration response of the systems under investigation, the following initial conditions were chosen in terms of generalized displacement $u_0 = 0.0$ m and velocity $\dot{u}_0 = 2.5$ m/s, whereas the generalized external force $p(t)$ is considered null. Figure 5a (Figure 5d) shows the time history of the various generalized work and energy components for system A (B). In both cases, it can be noted that:

(i) the generalized rate-independent work W_{ri} assumes negative values since the generalized rate-independent hysteretic force f_{ri} tends to bring the mass m back to its equilibrium position;

(ii) the reduction of the generalized mechanical energy E_M can be interpreted as an energy conservation process in which energy is converted into generalized internal energy E_I;

(iii) it can be noted that in the case of free vibrations, the entire amount of generalized mechanical energy, initially supplied to the system due to the initial conditions, has been converted into generalized internal energy through the rate-independent hysteretic phenomena, thus guaranteeing energy conservation;

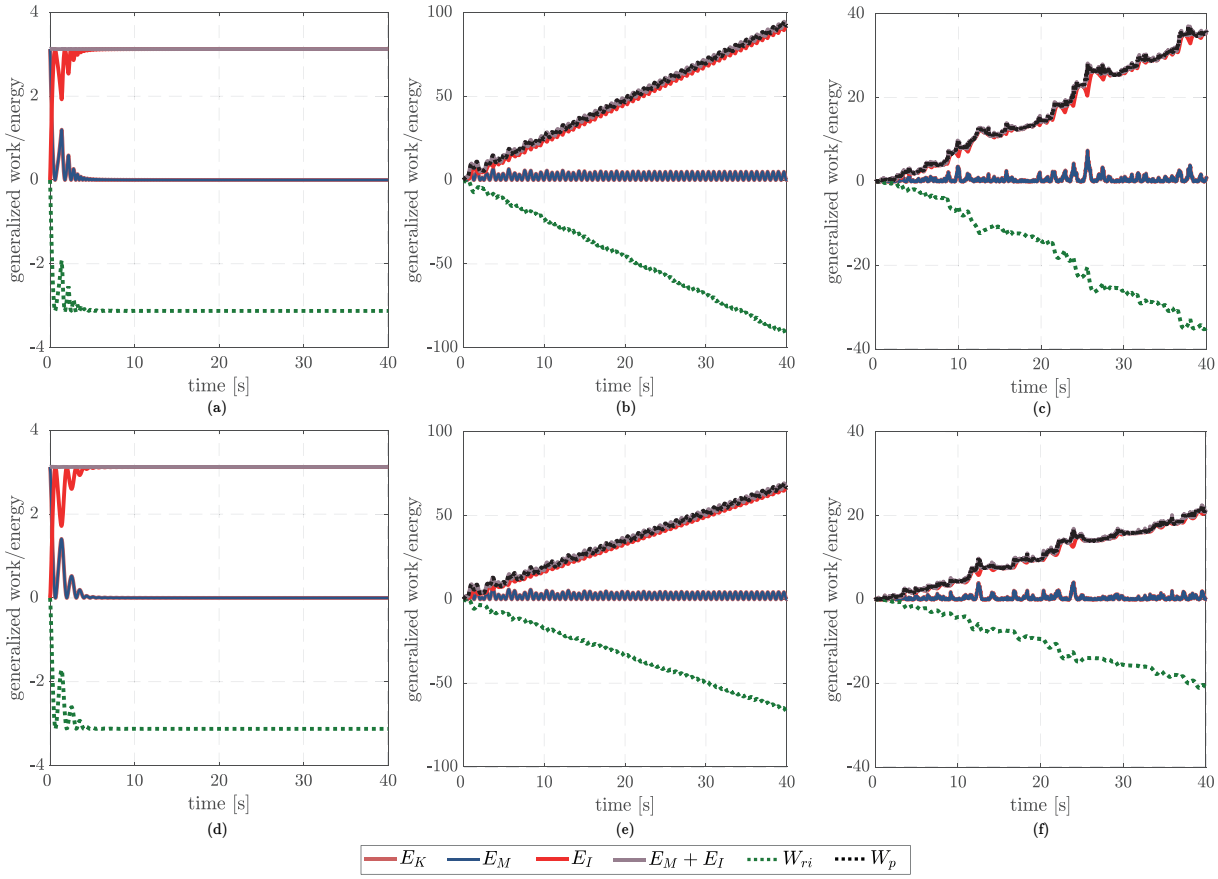

Figure 5: Time histories of the generalized energy and work components for the rate-independent hysteretic systems A (a, b, c) and B (d, e, f), obtained for free (a, d), forced harmonic (b, e) and forced random (c, f) vibrations.

(iv) since the generalized external force $p(t)$ is equal to zero, it can be deduced, from Equation (20), that the sum between generalized mechanical and internal energy $E_M + E_I$ is constant over time.

4.5.2 Forced harmonic vibrations

To evaluate the response of the system in the case of oscillations forced by a harmonic force, initial conditions of zero generalized displacements and velocity are imposed, whereas the load is assumed to be a harmonic function of the following type:

$$p(t) = p_0 \cos(2\pi f_p \, t), \tag{23}$$

where the amplitude is $p_0 = 10$ N and its frequency is $f_p = 0.75$ Hz. Figure 5b (Figure 5e) shows the time history of the various generalized work and energy components for system A (B). In both cases, it can be noted that:

(i) the motion of the mass m is caused by the generalized external work performed by the harmonic load that, as shown in the Figures 5b and 5e, is an increasing function over time;

(ii) the generalized mechanical energy and rate-independent work will no longer tend to an asymptotic value, as in the case of the free vibration, but they will assume values able to ensure fulfillment of the MWE theorem, i.e., Equation (20);

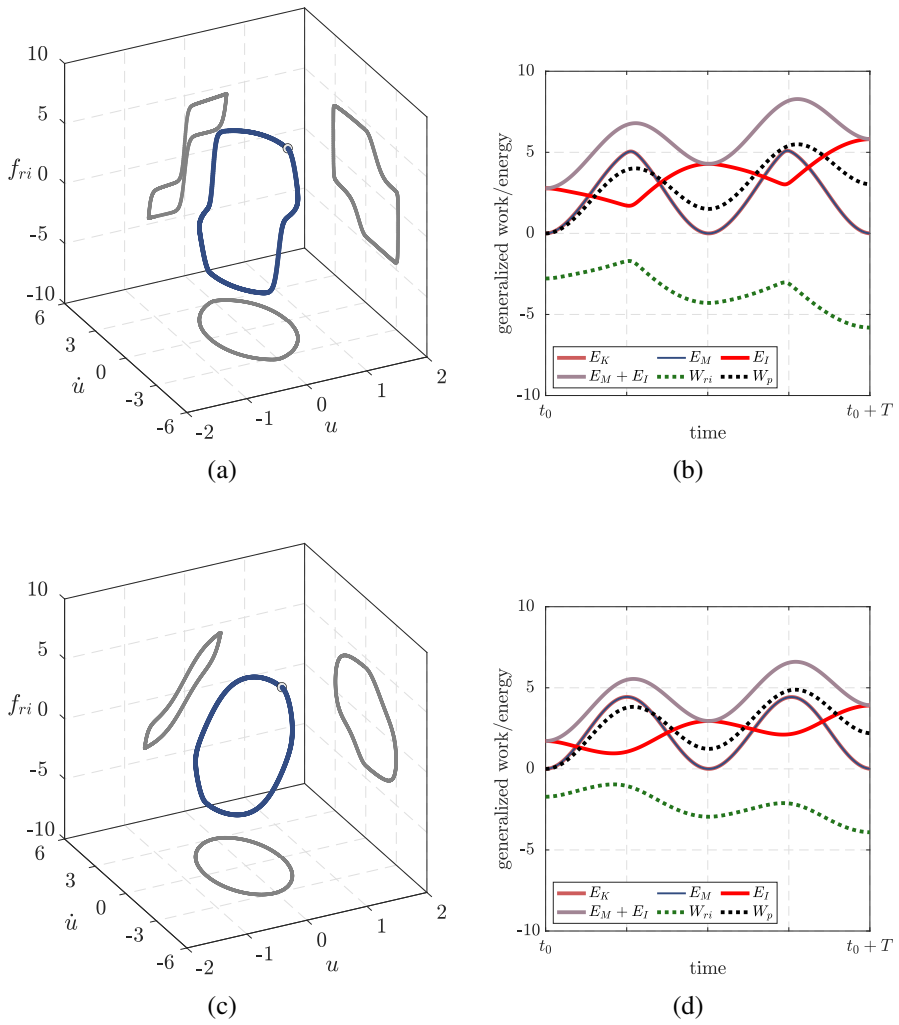

Figure 6: Steady-state response in the $(u, \dot{u}, f_{ri})$-state-space for the hysteretic mechanical system, and generalized work and energy components over a period T.

(iii) as a result of the chosen initial conditions, the sum between generalized mechanical and internal energy $E_M + E_I$ coincides with the generalized work done by the harmonic forcing W_p.

In this case, the time variation of the generalized mechanical energy E_M gives us precious information to distinguish the transition from a transient behavior, in which a reduction of the peaks of the generalized mechanical energy is observed, to a steady-state behavior [15].

Having determined the steady-state response of the two systems under consideration, a further analysis is performed, in which the initial conditions are chosen such that the system is in a steady-state response. In Figure 6 we can see the steady-state responses in the $(u, \dot{u}, f_{ri})$-state-space, with the relative projections for the two analyzed systems (Figures 6a and 6c), and time evolution of the generalized work and energy components over a period $T = \frac{1}{f_p}$ (Figures 6b and 6d).

4.5.3 Forced random vibrations

To evaluate the response of the system in the case of vibrations induced by a random load, initial conditions of zero generalized displacements and velocity are imposed, and a random

force modeled as a Gaussian white noise with a variance iwn $= 40$, is applied to the system as external force $p(t)$. Figure 5c (Figure 5f) shows the time history of the various generalized work and energy components for system A (B).

These latter cases are similar to the harmonic loading ones except for the distinction of transient and steady-state behaviors, which is not possible in this case since the load is not periodic.

5 CONCLUSIONS

We have used the MWE theorem to evaluate the generalized work and energy responses of different SDoF hysteretic mechanical systems with complex hysteresis loop shapes simulated by the VRM, in three particular cases: (i) free vibrations, (ii) forced harmonic vibrations and (iii) forced random vibrations. The performed analyses show valuable information on the time history of the generalized energy components of the systems under consideration, particularly in the case of the steady-state response of a harmonically forced system.

REFERENCES

[1] N. Vaiana, L. Rosati: Classification and unified phenomenological modeling of complex uniaxial rate-independent hysteretic responses. *Mechanical Systems and Signal Processing*, **182**, 109539, 2023.

[2] N. Vaiana, R. Capuano, L. Rosati: Evaluation of path-dependent work and internal energy change for hysteretic mechanical systems. *Mechanical Systems and Signal Processing*, **186**, 109862, 2023.

[3] R. Bouc: Modèle mathématique d'hystérésis. *Acustica*, **21**, 16-25, 1971.

[4] Y. K. Wen: Method for random vibration of hysteretic systems. *Journal of the engineering mechanics division*, **102**(2), 249-263, 1976.

[5] Y. K. Wen: Equivalent Linearization for Hysteretic Systems Under Random Excitation. ASME. *Journal of Applied Mechanics*, **47**(1): 150–154, 1980.

[6] R. Capuano, N. Vaiana, D. Pellecchia, L. Rosati: A Solution Algorithm for a Modified Bouc-Wen Model Capable of Simulating Cyclic Softening and Pinching Phenomena. *IFAC-PapersOnLine*, **55**(20), 319-324, 2022.

[7] I. Nuzzo, D. Losanno, N. Caterino, G. Serino, L. M. B. Rotondo: Experimental and analytical characterization of steel shear links for seismic energy dissipation. *Engineering Structures*, **172**, 405-418, 2018.

[8] A. Orfeo, E. Tubaldi, A. H. Muhr, D. Losanno: Mechanical behaviour of rubber bearings with low shape factor. *Engineering Structures*, **266**, 114532, 2022.

[9] D. Pellecchia, N. Vaiana, M. Spizzuoco, G. Serino, L. Rosati: Axial hysteretic behaviour of wire rope isolators: Experiments and modelling. *Materials & Design*, **225**, 111436, 2023.

[10] P. Zhuang, S. Xue, P. Nie, W. Wang: Experimental and numerical study on hysteretic performance of SMA spring-friction bearings. *Earthquake Engineering and Engineering Vibration*, **15**(4), 597-609, 2016.

[11] F. Cilento, D. Losanno, L. Piga: An experimental study on a novel reclaimed rubber compound for fiber-reinforced seismic isolators. *Structures*, **45**, 2022.

[12] D. Losanno, D. De Domenico, and I. E. Madera-Sierra: Experimental testing of full-scale fiber reinforced elastomeric isolators (FREIs) in unbounded configuration. *Engineering Structures*, **260**, 114234, 2022.

[13] D. De Domenico, D. Losanno, N. Vaiana: Experimental tests and numerical modeling of full-scale unbonded fiber reinforced elastomeric isolators (UFREIs) under bidirectional excitation. *Engineering Structures*, **274**, 115118, 2023.

[14] N. Vaiana, S. Sessa, F. Marmo, L. Rosati: Nonlinear dynamic analysis of hysteretic mechanical systems by combining a novel rate-independent model and an explicit time integration method. *Nonlinear Dynamics*, **98**, 2879–2901, 2019.

[15] G. Formica, N. Vaiana, L. Rosati, W. Lacarbonara: Pathfollowing of high-dimensional hysteretic systems under periodic forcing. *Nonlinear Dynamics*, **103**(4), 3515-3528, 2021.

Acknowledgments

The present work was performed in the framework of ReLUIS-DPC 2022-2024 Project (WP 15, Tasks 15.1 and 15.2) and in the context of the research activities carried out by the GNFM (Gruppo Nazionale per la Fisica Matematica).